Journal of Applied Fluid Mechanics, Vol. 17, No. 10, pp. 2228-2244, 2024.
Available online at www.jafmonline.net, ISSN 1735-3572, EISSN 1735-3645.
https://doi.org/10.47176/jafm.17.10.2482

Jet Array Design for the Physical Tempering Process of Ultrathin Glass

Z. Li [1], G. Cheng[1†], K. Zhu[2], Z. Zhang[1], J. Lin[3], J. Lin[3], and J. Ding[4]

[1] *Institute of Intelligent Flexible Mechatronics, Jiangsu University, Zhenjiang 212013, China*
[2] *Jiangsu Collaborative Innovation Center of Photovoltaic Science and Engineering, Changzhou University, Changzhou 213164, China*
[3] *Provincial Photoelectric Glass Key Laboratory, Changzhou Almaden Co., Ltd. Changzhou 213000, Jiangsu, China*
[4] *School of Mechanical Engineering, Yangzhou University, Yangzhou 225127, China*

†*Corresponding Author Email: ggcheng@ujs.edu.cn*

ABSTRACT

A high heat transfer rate and excellent heat transfer uniformity are crucial to the physical tempering manufacturing of glass. In the current study, numerical simulations were conducted to evaluate the influence of nozzle shape (circular, square, or triangular) on the transient heat transfer rate and uniformity during jet impingement heating using a square-array configuration at low nozzle-to-plate distances. The Reynolds number (*Re*) was varied between 2000 and 10000, the nozzle-to-plate distance to nozzle diameter ratio (*H/D*) was varied between 0.2 and 2, and the nozzle-to-nozzle spacing to nozzle diameter ratio (*S/D*) was set to values of 4, 5, and 7. The properties of heat transfer rate and uniformity are evaluated by the surface Nusselt number distribution, the average Nusselt number, and the coefficient of variation of temperature. The results revealed that a higher heat transfer rate and good heat transfer uniformity could be obtained only at *H/D* = 0.2 or 2. Furthermore, square and triangular nozzles afforded superior heat transfer rates and uniformity to the corresponding circular nozzles in specific jet configurations. Moreover, at low *H/D* values, non-circular nozzles can obtain a higher local maximum Nusselt number than circular nozzles, and significant axis switching occurs around the impingement hole in the center of the jet impingement wall.

Article History

Received December 6, 2023
Revised March 30, 2024
Accepted April 17, 2024
Available online July 31, 2024

Keywords:

Jet impingement
Nusselt number
Heat transfer rate
Heat transfer uniformity
Nozzle shape

1. INTRODUCTION

Jet impingement can effectively transfer enormous amounts of thermal energy or mass between a surface and a fluid by releasing a directed liquid or gas against the surface (Zuckerman & Lior, 2006; Ekkad & Singh, 2021). Jet impingement features the highest heat transfer rate among single-phase heat transfer methods and is widely used in a variety of thermal processing operations and thermal engineering equipment. Some common applications include the temperature control of glass and metal plates (Yu et al., 2017a; Zhu et al., 2018; Yang et al., 2022), preheating of billets (Ferrari et al., 2003), cooling of turbine blades (Yang et al., 2023), drying of paper, heating of furnaces, and cooling of combustion chambers (Xing & Weigand, 2013).

Previous research mainly focused on the steady-state jet impingement heat transfer using single holes, particularly for large nozzle-to-plate distance to nozzle diameter ratios (*H/D*). These studies consider the impact of various factors, such as the Reynolds number(*Re*) (Lytle & Webb, 1994; Jensen & Walther, 2013; Bhagwat & Sridharan, 2016; Zhang et al., 2020), nozzle-to-plate distance (Lytle & Webb, 1994; Yu et al., 2017a; Choo et al., 2016), jet diameter (Tang et al., 2020),nozzle shape (Singh et al., 2003; Zhao et al., 2004; Kim & Park, 2013; Vinze et al., 2016), jet temperature (Jensen & Walther, 2013; Vinze et al., 2016; Zhou et al., 2016), and jet medium (Nguyen et al., 2009; Yu et al., 2017b; Glaspell et al., 2019).

In recent years, photovoltaic cell modules have been evolving to become larger, lighter, more efficient, and less expensive. As a key auxiliary material for such modules, tempered glass must possess high transmittance, high strength, and an ultrathin profile. For the tempering of ultrathin glass, physical tempering has attracted substantial attention owing to its excellent tempering quality, lack of environmental pollution, and long tempering lifespan. The physical tempering process of

Nomenclature

D	diameter of the nozzle	S_k	user-defined source term
D_w	cross-diffusion term	S_w	user-defined source term
h	heat transfer coefficient	S_μ	Sutherland's constant for kinetic viscosity
H	nozzle to plate distance	T_{ave}	average temperature
I_t	total enthalpy	T_r	reference temperature
K_{air}	thermal conductivity of air	u	fluid velocity
T	use the "Tab" key to add more rows to this table	ρ	density
$\dot{m}$	mass flow rate of jets	λ	thermal conductivity
Nu	Nusselt number	λ_r	Reference thermal conductivity
$\overline{Nu}$	average Nusselt number	$\vec{\tau}$	stress tensor
p	static pressure	μ	dynamic viscosity
R	gas constant of air	Γ	effective diffusivity
R_0	ideal gas constant	air	air
Re	Reynolds number	ave	average
S	nozzle to nozzle spacing		

ultrathin glass entails heating the glass with high-temperature air and then quenching it to induce compressive stress on the glass surface, thereby enhancing its strength. It is noteworthy that uneven heat transfer during the glass tempering heating phase can cause warping deformation, affecting surface quality and reducing heat transfer efficiency, making it difficult to achieve the desired stress distribution of compressive stress on the surface and tensile stress in the interior. Moreover, the ultrathin nature (≤1.6 mm) of the glass needed for photovoltaic cell modules imposes strict requirements on the heat transfer rate and uniformity of the impinging jet during the heating process. Compared with jet heating equipment designed for other working scenarios, the array jet arrangement is more suitable for large-area heating. In the impinging jet heating bins for the physical tempering of glass (Yazici et al.,2015), the jet medium is air at 953 K. This leads to a significant temperature difference between the jet medium and the glass plate, with the heat transfer exhibiting pronounced time dependence. Moreover, owing to the short distance between the nozzles and the plate, which is only a few millimeters, it becomes imperative to investigate the transient heat transfer rate and uniformity under conditions of high-temperature differentials and small nozzle-to-plate distances in the array jet heating process.

Numerous scholars have conducted extensive research into heat transfer during array jet impingement. For example, San and Chen (2014) carried out an experimental study on circular nozzle jet impingement, considering different nozzle-to-nozzle spacing to nozzle diameter ratios(*S/D*) ranging from 2 to 8 and nozzle-to-plate distances (*H/D*) ranging from 0.5 to 3. Their findings demonstrated that *S/D* is the primary factor influencing heat transfer inhomogeneity, while *H/D* is a secondary factor. Singh et al. (2021) studied the jet impingement heat transfer properties of a square array of nine jet holes for the condition of *H/D*≥6 by numerical simulation. Culun et al. (2018) performed simulations of synergistic heat transfer for multi-jet impingement and determined that the jet arrangement is the weakest parameter affecting heat transfer. San and Lai (2001) as well as Singh and Prasad (2020) proposed novel configurations, namely, an equidistant staggered jet arrangement and an equidistant staggered jet arrangement with chamfered nozzles, respectively. Siw et al. (2016) examined the heat transfer performance of single-row jet impingement cooling under different flow rates with *H/D*=2. The results revealed that increasing the total flow rate by approximately 65% led to a heat transfer augmentation of about 35% on the target surface. Interestingly, previous studies on array jet impingement primarily concentrated on impingement cooling with large *H/D* values (≥1), with little attention devoted to high-temperature jets.

In addition, Ikhlaq et al. (2019) compared the transient jet development for a single hole under rotating and non-rotating conditions using high-resolution time-series infrared imaging data. Vinze et al. (2016) researched the influence of nozzle shape for a single hole on the local heat transfer distribution and efficiency at different jet heights with *H/D*≥1. In comparison to square and triangular nozzles, circular nozzles exhibited the highest heat transfer rate. Singh et al. (2003) carried out an experimental investigation on the entrainment characteristics of confined/semiconfined circular and noncircular jets. The results revealed that isosceles triangular jets displayed the highest entrainment among confined jets, with an entrainment rate that was nearly 10% greater than that of circular jets. Zhao et al. (2004) studied single-hole jets with various nozzle shapes at *H/D* values ranging from 2 to 8. Noncircular nozzles were found to exhibit enhanced heat transfer only at lower *H/D* values. Attalla et al. (2017) investigated the effect of circular and square nozzles on the heat transfer uniformity of an in-line array jet impinging on a smooth plane with a large separation distance (2≤*H/D*≤8). It was discovered that circular nozzles resulted in an average Nusselt number 7.8% higher than that of square nozzles. Furthermore, the heat transfer uniformity for square nozzles exceeded that for circular nozzles by 10.45%. The above studies indicated that within the range of nozzle-to-plate distances examined, non-circular jets at low *H/D* values exhibit superior heat transfer performance. Therefore, to optimize both heat transfer uniformity and rate, it is necessary to explore the influence of jet impingement transient heat

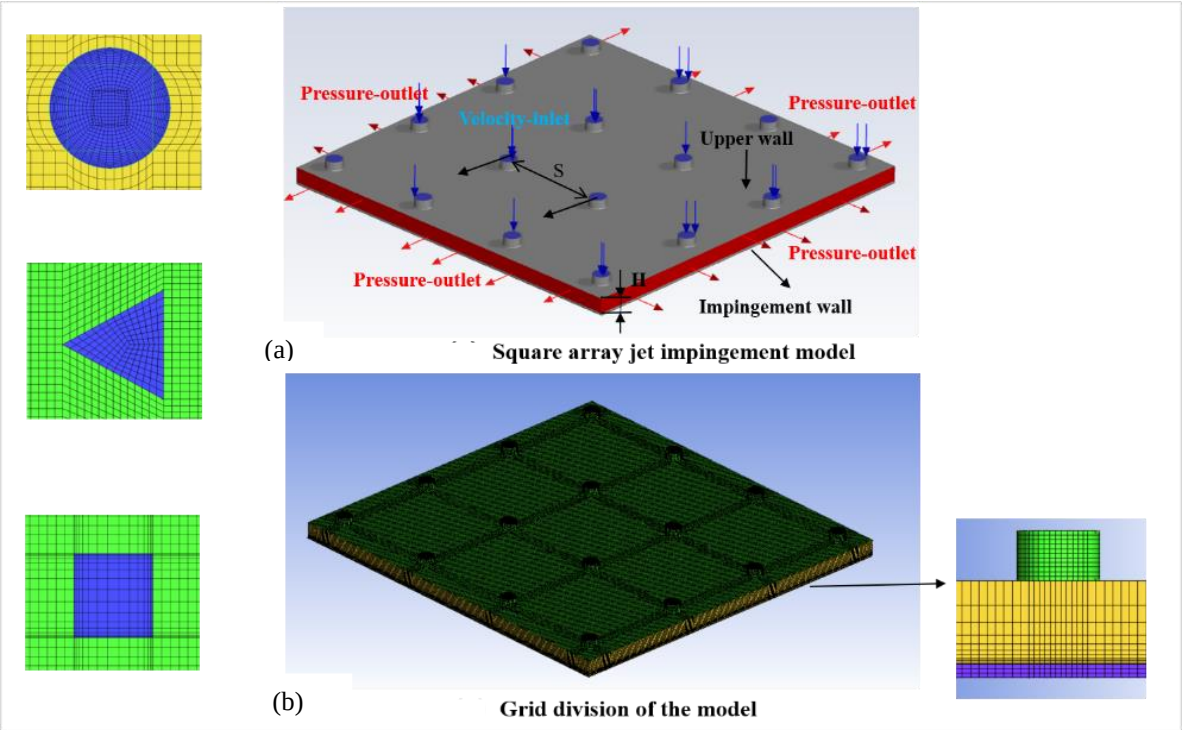

Fig. 1 Square array jet impingement model and meshing

transfer for different nozzle shapes (circular, square, and triangular) at lower *H/D*.

Through the above literature survey, we find that there is no information available on the transient heat transfer rate and uniformity of array jet impingement for different nozzle shapes. However, especially at low nozzle-to-plate distances, non-circular nozzles can provide better heat transfer characteristics. In our paper, we examined the transient heat transfer rate and uniformity during square-array jet impingement using different nozzle shapes (circular, square, and triangular) at low nozzle-to-plate distances with a large temperature difference. Numerical simulations were performed with *Re* values ranging between 2000 and 10000. Additionally, the *H/D* values range from 0.2 to 2, the *S/D* values are set at 4, 5, and 7 under a constant mass flow rate. The obtained results provide theoretical support for the design of gas suspension heating bins for the physical tempering of ultrathin glass.

2. GEOMETRY AND NUMERICAL SIMULATION

2.1 Square Array Jet Impingement Model

Figure 1(b) shows a model of the square-array jet impingement for various nozzle shapes. The equivalent diameters (D) of the non-circular nozzles were calculated by equating their cross-sectional areas to that of a circular cross-section. The equivalent diameter for all nozzles in the jet model was 10 mm, and the height was 6 mm. In this work, we examined *Re* values ranging between 2000 and 10000. At a certain mass flow rate, the effects of *H/D* values ranging from 0.2 to 2 and *S/D* values of 4, 5, and 7 were evaluated. In a typical physical tempering for ultrathin glass (Yu et al., 2017a), the spacing between the jet nozzle(s) and the target glass plate is extremely small (several millimeters), which is why we chose to investigate *H/D* values of 0.2–2. In the experimental study by San and Chen (2014), the interactions and interference effects between jets were weak when $S/D \geq 4$, and each jet formed an independent cooling zone on the target plate when $S/D \geq 6$. Similarly, Huber and Viskanta (1994) reported that the maximum average heat transfer on the jet target plate occurred at S/D=4. Given these findings, we selected *S/D* values of 4, 5, and 7 to explore the heat transfer characteristics within this range. Zhao et al. (2004) and Attalla et al. (2017) studied the jets produced by various nozzle shapes with *H/D* values ranging from 2 to 8 and found that non-circular nozzles exhibited superior heat transfer characteristics at lower *H/D* values. Therefore, we investigated the heat transfer characteristics of circular, square, and triangular jets at low nozzle-to-plate distances. The specific jet nozzle arrangements are illustrated in Fig. 2. The jet impingement plate an ultrathin smooth glass plate of 1.6 mm thickness with a fixed density of 2.5×10^3 kg/m^3. The thermal properties of glass change significantly with increasing temperature, and we calculated the temperature-dependent standard thermophysical properties, including the specific heat and thermal conductivity, for the ultrathin glass plates.

During the physical tempering of glass, it is necessary to heat the glass to its softening temperature (950–960 K), for which high-temperature air at 953 K is a typical jet medium. It is worth noting that, as shown in previous studies, the density and thermal properties of air undergo significant changes at high temperatures (Zhou et al., 2016). Compared with heat transfer at lower temperatures, these changes have a greater impact on the heat transfer process. We assume that the flow is incompressible, and the density and thermal properties are

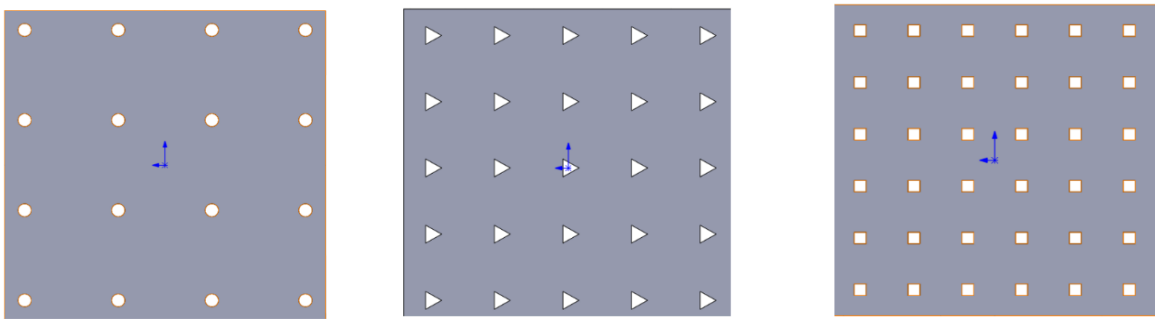

Fig. 2 The arrangement of the jet nozzle

considered to only vary with temperature. The *Re* value was calculated from the total mass flow rate ($\dot{m}$) and high-temperature gas properties using the following formula:

$$\mathrm{Re}=\frac{\rho Dv}{\mu}=\frac{4\dot{m}}{n\pi\mu D} \tag{1}$$

Where ρ is the density, and D is the equivalent diameter of the nozzle，n is the number of nozzles. We used Eq. (1) to obtain the incident *Re* value for the high-temperature gas considered in this paper based on the total mass flow rate of ambient air at room temperature reported by Yu et al. (2017a) and Yazici et al.(2015) for impingement cooling during glass physical tempering .

The density was calculated using the equation of state for an incompressible ideal gas:

$$P=\rho\frac{R_0}{M}T \tag{2}$$

where p is the pressure, R_0=8.314 J/(mol·K), M is the molar mass of the gas, and T is the gas temperature.

The equation of state for air can be shortened to the following:

$$P=\rho RT \tag{3}$$

where R is the gas constant of air.

The dynamic viscosity (μ) and thermal conductivity (λ) were calculated using Sutherland's law:

$$\mu=\mu_r\left(\frac{T}{T_r}\right)^{3/2}\frac{T_r+S_\mu}{T+S_\mu},\lambda=\lambda_r\left(\frac{T}{T_r}\right)^{3/2}\frac{T_r+S_\lambda}{T+S_\lambda} \tag{4}$$

where T_r is the reference temperature (273.15 K), μ_r is the dynamic viscosity at the reference temperature, S_μ is the Sutherland constant for dynamic viscosity, λ_r is the thermal conductivity at the reference temperature, and S_λ is the Sutherland constant for thermal conductivity.

A geometric model for grid partitioning was established using the ICEM software, defining fluid domain and solid domain blocks. To improve grid quality, we perform O-block partitioning on circular nozzles in the fluid domain, Y-block tangents on triangular nozzles, and a regular hexahedron structure on solid domains. In order to better capture fluid phenomena and temperature gradients near the wall, the mesh at the nozzle inlet and the fluid-solid connection in the convective domain were refined, as shown in Fig. 1(b). In the near-wall region, we maintained a maximum wall-normal spacing of y+=0.72, with a wall-normal expansion ratio of 1.1.

2.2 Control Equations and Boundary Conditions

2.2.1 Control Equations

The established numerical heat transfer model for jet impingement was used to solve the energy equation, continuity equation, and momentum equation given in Eqs. (5)–(7), and computational fluid dynamics (CFD) simulations were then performed to examine the jet impingement characteristics for square arrays with different nozzle shapes.

Continuity equation:

$$\frac{\partial\rho}{\partial t}+\nabla(\rho u)=0 \tag{5}$$

Momentum equation:

$$\frac{\partial(\rho u)}{\partial t}+\rho(u\cdot\nabla)u=\nabla p+\nabla\vec{\tau} \tag{6}$$

Energy equation:

$$\frac{\partial(\rho I_t)}{\partial t}+\nabla\left((\rho I_t+p)u\right)=\nabla\left(k\nabla T+\left(\bar{\tau}\cdot U\right)\right) \tag{7}$$

Here, ρ is the density, P is the pressure, λ is the thermal conductivity, u is the velocity, $\bar{\tau}$ represents the stress tensor, and I_t denotes the total enthalpy.

Numerous researchers have chosen to use the k–ω turbulence model because of its low computational cost and the consistency of the simulation results with jet impingement theory. In the present work, this model was employed in conjunction with the shear stress transfer (SST) model. This combination is better suited for handling the computational process of near-wall flow, offering wide practicality and high computational accuracy. The relevant flow equations are as follows:

$$\frac{\partial(\rho k)}{\partial t}+\frac{\partial(\rho k u_j)}{\partial x_j}=\frac{\partial}{\partial x_j}\left(\Gamma_k\frac{\partial k}{\partial x_j}\right)+G_k-Y_k+S_k \tag{8}$$

$$\frac{\partial(\rho w)}{\partial t}+\frac{\partial\left(\rho w u_j\right)}{\partial x_j}=\frac{\partial}{\partial x_j}\left(\Gamma_w\frac{\partial w}{\partial x_j}\right)+G_w-Y_w+D_w+S_w \quad (9)$$

Here, Γ_k and Γ_w are turbulent diffusion terms, G_k and G_w are terms representing turbulent kinetic energy production, Y_k and Y_w are turbulent dissipation rates, and S_k and S_w are source terms.

2.2.2 Boundary Conditions

In the heating process of ultra-thin glass, there is a characteristic of small nozzle-to-plate distance and thin glass. Therefore, only the influence of convective heat transfer was considered during the simulations, while the effects of heat conduction and thermal radiation were neglected.

At the nozzle inlet, a velocity inlet boundary condition was imposed, and the hot air flow impinged on the glass plate, where the gas was considered incompressible and the inlet temperature was 953 K. The upper wall of the fluid domain and the nozzle surface were assumed to possess an adiabatic no-slip boundary. A pressure outlet boundary condition was applied at the jet outlet, where the system pressure was 1 atm. The liquid–solid interface (impingement wall) was set as a coupled conjugate heat transfer boundary. Convective heat transfer boundary conditions were used on the outer surface of the glass to handle the heat transfer between the hot air flow and the glass surface. In addition, we established an initial boundary condition with the glass temperature assumed to be 298 K at the outset (t=0 s).

2.3 Numerical Simulation

CFD simulations were conducted using the Ansys Fluent software (2021 R2). The SIMPLE algorithm was employed to solve the pressure and velocity coupling. To improve the calculation accuracy, various physical quantities such as turbulence kinetic energy, laminar kinetic energy, specific dissipation rate, momentum, and energy were chosen in the second-order upwind scheme. In this work, the SST k–ω model was used to obtain more precise results.

In previous studies, Lee et al., (2013) conducted an in-depth investigation into the effect of the nozzle-to-plate distance and *Re* value on the heat transfer during array jet impingement, with a particular focus on using the average Nusselt number at the surface to elucidate the heat transfer effectiveness. Furthermore, Yu et al., (2017b) quantitatively described the heat transfer uniformity during mist flow jet impingement on glass plates using the standard deviation percentage of the Nusselt number at the surface. Similarly, Bijarchi et al. (2019) used the standard deviation to evaluate the heat transfer uniformity, and Huber and Viskanta (1994) examined the local Nusselt numbers to reveal the (non-)uniformity of heat transfer.

We adopted the average Nusselt number ($\overline{Nu}$) as a metric to evaluate the jet impingement heat transfer rate. However, given that we are studying transient properties, wherein different samples concurrently exhibited varying average temperatures, assessment of the standard deviation appeared unsuitable. Therefore, to consider the transient heat transfer uniformity during the heating process, we utilized the coefficient of variation of temperature (σ_{T,t_j}) to quantitatively evaluate the differences in average values. Furthermore, the surface Nusselt number (*Nu*) distribution was utilized to elucidate the uniformity of heat transfer. These calculations were performed using the following equations:

$$Nu=\frac{hD}{K_{air}},\overline{Nu}=\sum_{i=1}^{n}\frac{Nu_i}{n} \quad (10)$$

$$T_{ave,t_j}=\sum_{i=1}^{n}\frac{T_{i,t_j}}{n},\sigma_{T,t_j}=\frac{\sqrt{\frac{1}{n}\sum_{i=1}^{n}\left(T_{i,t_j}-T_{ave,t_j}\right)^2}}{T_{ave,t_j}} \quad (11)$$

Here, K_{air} is the thermal conductivity of air, h is the convective heat transfer coefficient, σ_{T,t_j} is the coefficient of variation of the surface temperature at the moment of t_j, and T_{ave,t_j} is the average surface temperature at the moment of t_j.

3. VERIFICATION OF GRID INDEPENDENCE

To check the grid independence in the numerical calculation of the jet impingement model, simulations are performed for the circular jet array impingement model with *S/D* = 7 and *H/D* = 1. The corresponding results are presented in Fig. 3, which compares the obtained $\overline{Nu}$ values at the impingement wall as a function of heating time for three refinement grids. By considering three refinement meshes with different numbers of cells, i.e., 991772 (Mesh 1), 1336928 (Mesh 2), and 1714641 (Mesh 3), it was found that the maximum difference between the predicted results occurred in the early stages of heating. The maximum difference between Mesh 2 and Mesh 3 was only 1.9%, while that between Mesh 1 and Mesh 3 was 6.3%. Therefore, Mesh 2 was considered to provide sufficient computational domain resolution without excessive computational expense, and it was thus used in the subsequent simulations.

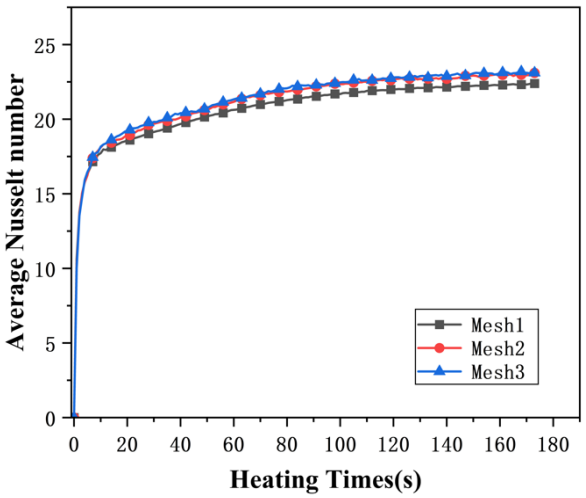

Fig. 3 Verification of grid independence

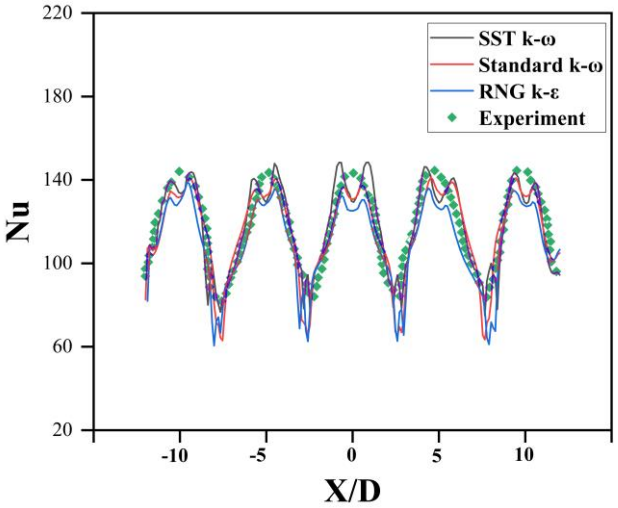

Fig. 4 Comparison of the predicted local Nusselt number distributions with experimental data

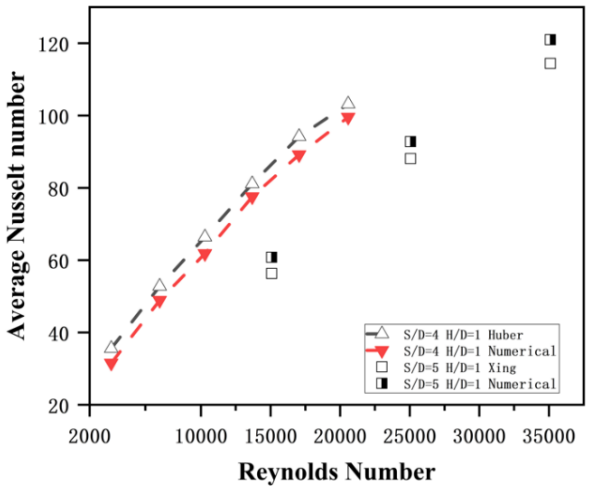

Fig. 5 Comparison between the results of the numerical model and experiment data

4. VALIDATION OF SST "K-Ω" MODEL

To evaluate the performance of the SST "k-ω" turbulence model, the predicted fluid properties and heat transfer characteristics of circular nozzles were compared with experimental data obtained from Ichikawa et al. (2016), Xing and Weigand (2013), and Huber and Viskanta (1994) for a square-array jet impinging on a flat plate. Ichikawa et al. (2016) made a visual experimental study of the square-array jet impingement model and proposed a normalized analysis of V_R , representing the maximum roll-up velocity of fluid impact. The numerical simulation result for the jet configuration with S/D = 4 and H/D = 2 was compared with experimental results (V_R). The value obtained from the simulation was 0.5073, which was found to have a relative error of only 5.4% when compared to the experimental data.

Different structures have varying adaptability to turbulence modeling, and other turbulence models (Standard k-ω and RNG k-ε) are also widely used to study the heat transfer performance during jet impingement. To evaluate the effectiveness of the SST k–ω turbulence model, we compared three turbulence models with the experimental square-array jet impingement heating data reported by Xing and Weigand (2013), as shown in Fig 4. The results revealed that the SST *k–ω* turbulence model was in good agreement with the experimental results, and it performed particularly well in capturing the secondary peak of the surface *Nu* values, with a maximum error of only 7.9%.

Moreover, to further validate the accuracy of the numerical findings, we compared the average Nusselt numbers acquired at different Reynolds numbers under H/D = 1 with the experimental results of Xing and Weigand (2013) and Huber and Viskanta (1994), as illustrated in Fig.5. For these previous experimental results of vertically square-array jet impingement heating, we employed numerical model settings with the same boundary conditions as their experimental setup. The results depicted in Fig.5 reveal strong agreement between the average Nusselt numbers computed using the SST k-ω turbulence model and the experimental data. The numerical data exhibited a maximum deviation of merely 8% when compared to the findings of Xing and Weigand (2013). In comparison to the experimental results of Huber and Viskanta (1994), thus the numerical results exhibit a maximum deviation of 12.7%, underestimating the $\overline{Nu}$ in that region. This discrepancy can be attributed to the fact that the experimental setup by Huber and Viskanta (1994) featured an increased heat transfer rate due to the configuration of the spent air exit. These validation results indicate that the predictions obtained from the SST *k–ω* turbulence model can be considered plausible, and all of the results presented below were obtained using this numerical model.

5. RESULTS AND DISCUSSIONS

In this work, the effects of variations in *S*/*D*, *H*/*D*, and *Re* on the heat transfer rate and uniformity were numerically studied for different nozzle shapes. The jet configurations employed are listed in Table 1.

5.1 Research on Transient Heat Transfer Rate

The transient average Nusselt number plots for different nozzle shapes at Re ranging from 2000 to 10000, with *S*/*D*=7 and *H*/*D*=0.2 are given in Fig. 6. The current results are compared with the transient single-hole heat transfer research conducted by Ikhlaq et al. (2019) and Yu et al. (2017a). A similar trend in the variation of $\overline{Nu}$ with heat transfer time was observed during square-array jet impingement. However, the distinction lies in our focus on array jet impingement at high temperatures. At *H*/*D*=0.2, irrespective of the nozzle shape, the array jet heating process with a large temperature difference exhibited a rapid increase in $\overline{Nu}$ during the initial 20 s of heating. As the jet heating continued, $\overline{Nu}$ gradually reached a stable value. This behavior was primarily attributable to the large temperature difference between the hot air and the glass plate during the early stages of heating, resulting in a rapid increase in $\overline{Nu}$. However, as the glass plate approached a certain temperature, the rate of increase in $\overline{Nu}$ slowed

Table 1 Square array jet impingement configuration

$\dot{m}(kg/h)$	*Re*	*Shape*	*S/D*	*H/D*
68.36	1620	○、□、△	4	0.2、0.4、0.6、0.8、1、2
68.36	2330	○、□、△	5	0.2、0.4、0.6、0.8、1、2
68.36	3640	○、□、△	7	0.2、0.4、0.6、0.8、1、2
37.56	2000	○、□、△	7	0.2
75.12	4000	○、□、△	7	0.2
112.68	6000	○、□、△	7	0.2
150.24	8000	○、□、△	7	0.2
187.8	10000	○、□、△	7	0.2

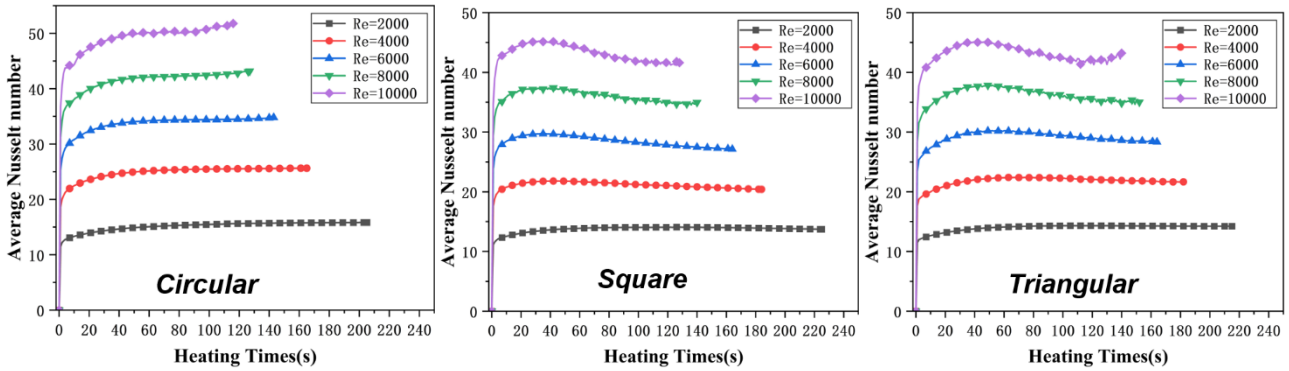

Fig. 6 Study of the transient $\overline{Nu}$ for different nozzle shapes at different Re

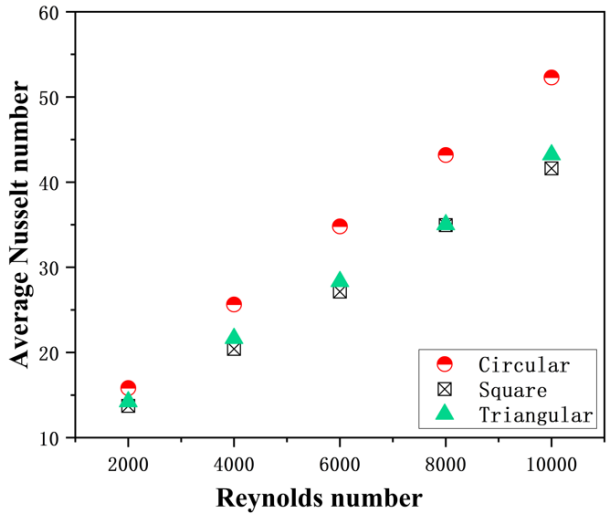

Fig. 7 $\overline{Nu}$ of different jet configurations when reaching the heating temperature of the glass plate at different Re

down, leading to lower heating efficiency in the later stages compared with the earlier stages.

As observed in Fig.7, the circular nozzles consistently achieved higher $\overline{Nu}$ values compared with the square and triangular nozzles, especially at larger *Re* values. This difference in performance can be ascribed to the higher decay rate of axial velocity reported by Kim and Park (2013) and Vinze et al. (2016) for square and triangular nozzles. Consequently, non-circular jets experience weaker interaction and lower local turbulence intensity, resulting in a lower efficiency of jet impingement.

Furthermore, when *Re*≥4000, the effect of the nozzle shape on the heat transfer rate became more pronounced.

At the lower *Re* value of 2000, the three nozzle shapes afforded similar $\overline{Nu}$ values, which is consistent with the findings reported by Attalla et al. (2017). The difference lies in the fact that our study was conducted at small nozzle-to-plate distances. In addition, $\overline{Nu}$ exhibited a linear relationship as *Re* increased, indicating a pronounced enhancement of the heat transfer rate with increasing *Re*. This enhancement arises from the augmentation of *Re*, denoting an intensified jet velocity, which in turn leads to an increase in turbulent kinetic energy within the wall jet region.

At a certain mass flow rate, studies of heat transfer rate for different nozzle shapes under different *H/D* and *S/D* are shown in Fig.8. Moreover, Fig. 9 shows the $\overline{Nu}$ values when the required heating temperature (950 K) of the glass plate was attained under different jet configurations. Notably, the transient change trend of $\overline{Nu}$ was consistent for the non-circular and circular jets. At the

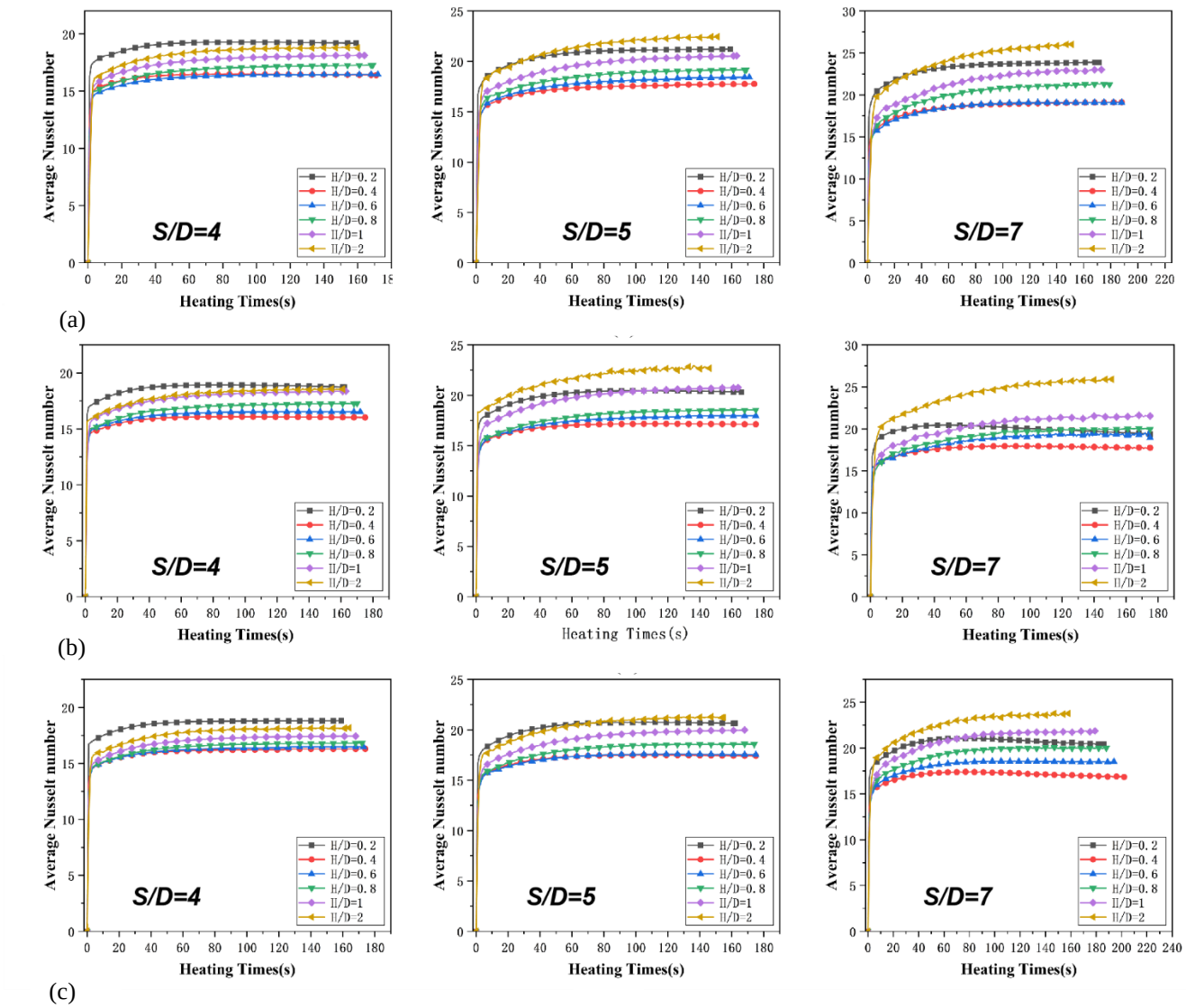

Fig. 8 Study of the transient $\overline{Nu}$ for different nozzle shapes at fixed flow rate: "*S/D*" for 4, 5, 7, "*H/D*" for 0.2-2 (a), circular (b), square (c), triangular

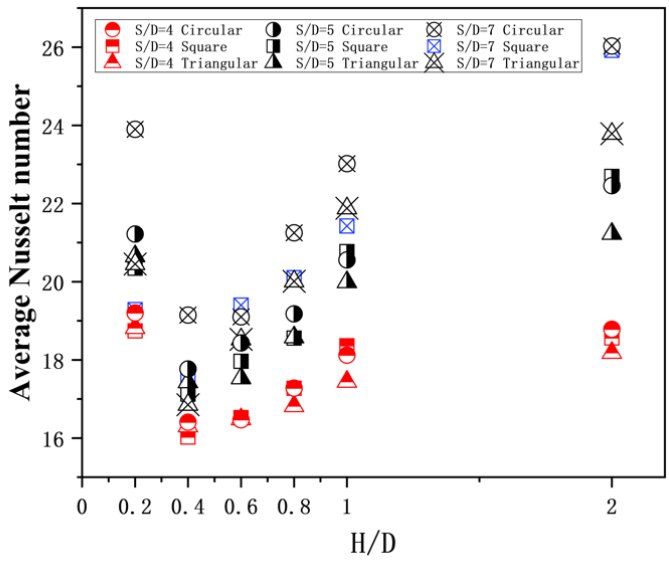

Fig. 9 $\overline{Nu}$ of different jet configurations when reaching the heating temperature of the glass plate

Table 2 Studies of for different jet configurations

Shape	*S/D*	Inflection point of $\overline{Nu}$ for *H/D*	Inflection point of σ_T for *H/D* (100s)	Optimal heat transfer uniformity for *H/D*
○	4	0.4	0.8	0.2
	5	0.4	0.4	2
	7	0.4	0.4	2
□	4	0.4	0.6	2
	5	0.4	0.6	2
	7	0.4	0.8	2
△	4	0.4	0.8	0.2
	5	0.4	0.8	2
	7	0.4	0.4	2

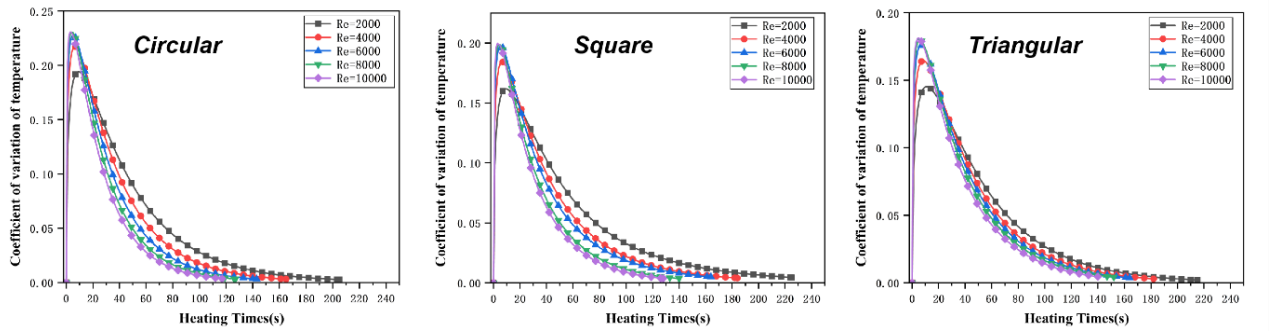

Fig. 10 Study of the transient coefficient of variation of temperature for different nozzle shapes at different *Re*

same *S*/*D* value, as *H*/*D* increased from 0.2 to 2, the $\overline{Nu}$ value at the impingement wall first became smaller and then increased, with the inflection point occurring at *H*/*D*=0.4. This inflection point was also reported by Yu et al. (2017a) and Glaspell et al. (2019) in their research, which focused on single-hole circular jet flows with small nozzle-to-plate distances. The appearance of this inflection point can be attributed to the jet deflection effect, leading to changes in the flow field structure, flow intensity, and vortex positions with varying jet heights. From our examination of the inflection points of $\overline{Nu}$ in Table 2, we note that the influence of the nozzle shape and jet array was minor.

At a certain mass flow rate, $\overline{Nu}$ decreased with decreasing *S*/*D* (the number of nozzles increases). This was attributable to the increase in the number of nozzles, which requires a reduction in *Re* to maintain a consistent inlet flow rate. Although the interaction between jets may become stronger in relative terms, it overall weakens the turbulence intensity within the confined impinging jets. When *S*/*D*=4, which means that the nozzles were arranged too closely, $\overline{Nu}$ reached its maximum value at *H*/*D*=0.2, resulting in the maximum heat transfer rate. At *S*/*D*≥5, the heat transfer rate was highest when *H*/*D*=2, although a high heat transfer rate was still attained at *H*/*D*=0.2, which was second only to the case of *H*/*D*=2. This was attributable to the more pronounced jet deflection effect and increased turbulence intensity within the wall–jet region under *H*/*D*=0.2. Compared with the study for *H*/*D*≥2 reported by Attalla et al. (2017), it is evident that a superior heat transfer rate could always be achieved irrespective of the nozzle shape at an extremely small nozzle-to-plate distance (*H*/*D*=0.2).

Therefore, at a certain mass flow rate, the circular nozzles generally afforded a better heat transfer rate than the non-circular nozzles. The triangular nozzles exhibited the poorest heat transfer rate, and the difference became more noticeable as *S*/*D* increased. At small nozzle-to-nozzle spacings (*S*/*D*=4 or 5), the non-circular nozzles displayed heat transfer rates comparable to the circular ones at short nozzle-to-plate distances (*H*/*D*≤1), with a maximum difference of only 3.8%. This minor difference can be ascribed to the fact that the higher axial velocity decay rate of non-circular nozzles does not significantly influence the heat transfer rate at smaller *Re* values. Moreover, the heat transfer rate was slightly better for the triangular jets than for the square ones at small nozzle-to-plate distances (*H*/*D*≤0.4), which can be attributed to the stronger three-dimensional development of triangular jets (Kim & Park, 2013). The heat transfer rate for the square nozzles at *S*/*D* values of 4 and 5 and larger nozzle-to-plate distances (1≤*H*/*D*≤2) was slightly superior to that for the circular nozzles, with a maximum difference of only 2.3%. Notably, $\overline{Nu}$ did not vary significantly for 0.4≤*H*/*D*≤0.8 in the jet configurations with smaller nozzle-to-nozzle spacings (*S*/*D*=4 or 5), which indicates that it is difficult to obtain a good heat transfer rate for these configurations.

5.2 Research on Transient Heat Transfer Uniformity

Figures.10, 11, 12, and 13 demonstrate the study of transient heat transfer uniformity on the impingement wall, which was evaluated using the coefficient of variation of temperature (Eq. (11)). As observed in Fig. 10,

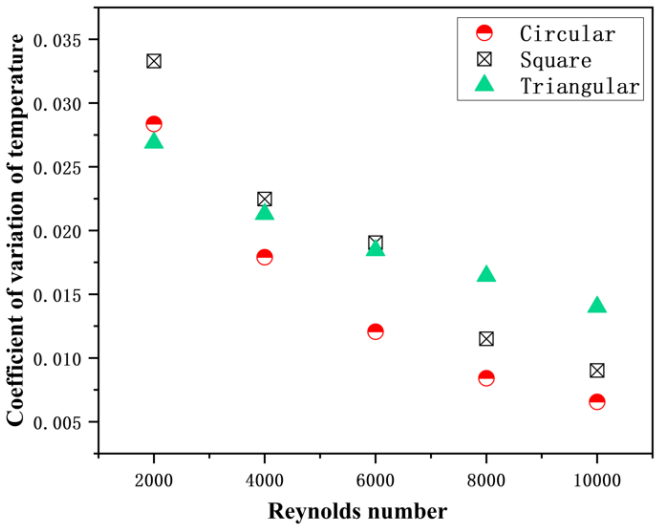

Fig. 11 The magnitude of the coefficient of variation of temperature at the late stage of heating (100s) at different *Re*

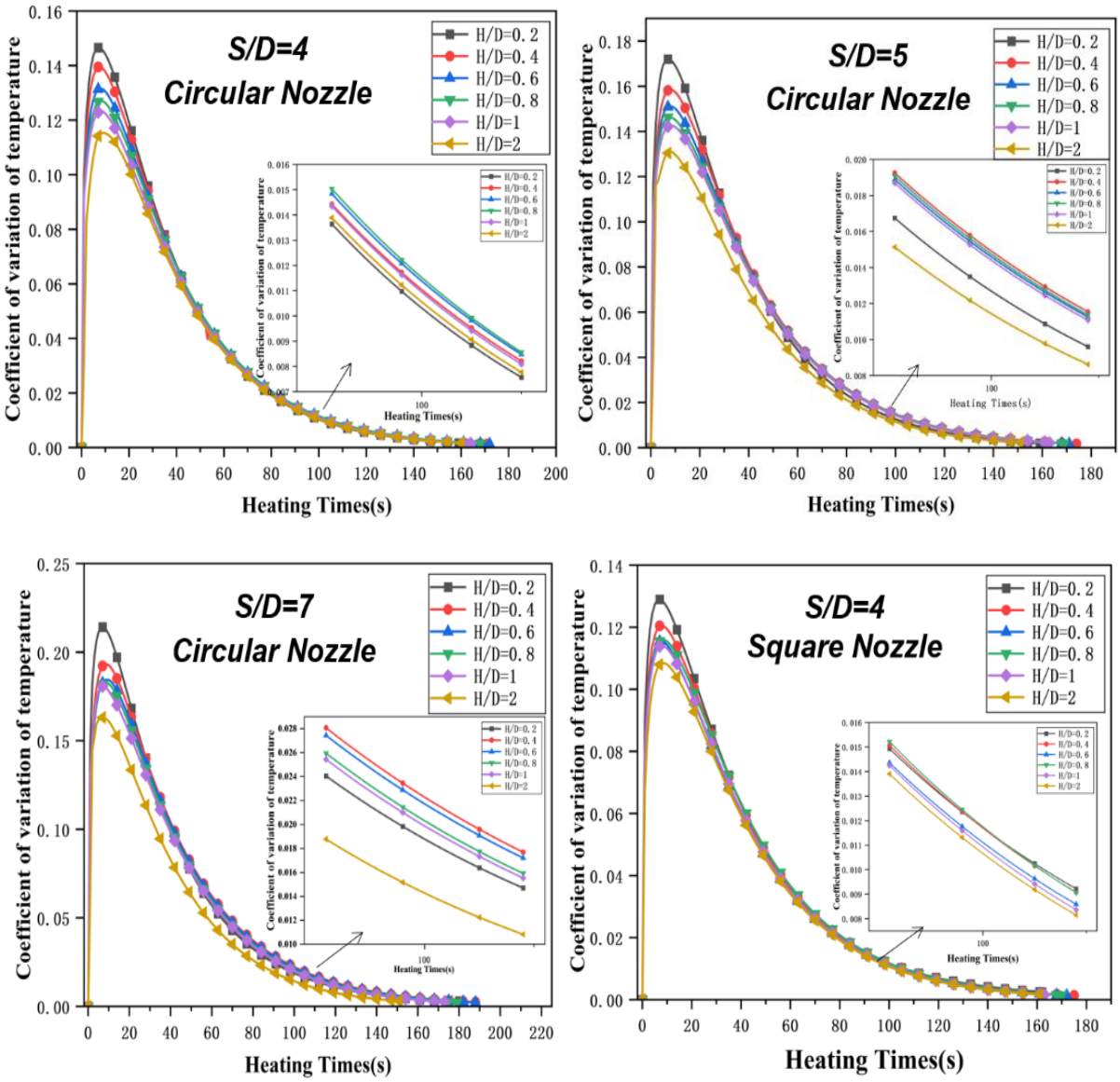

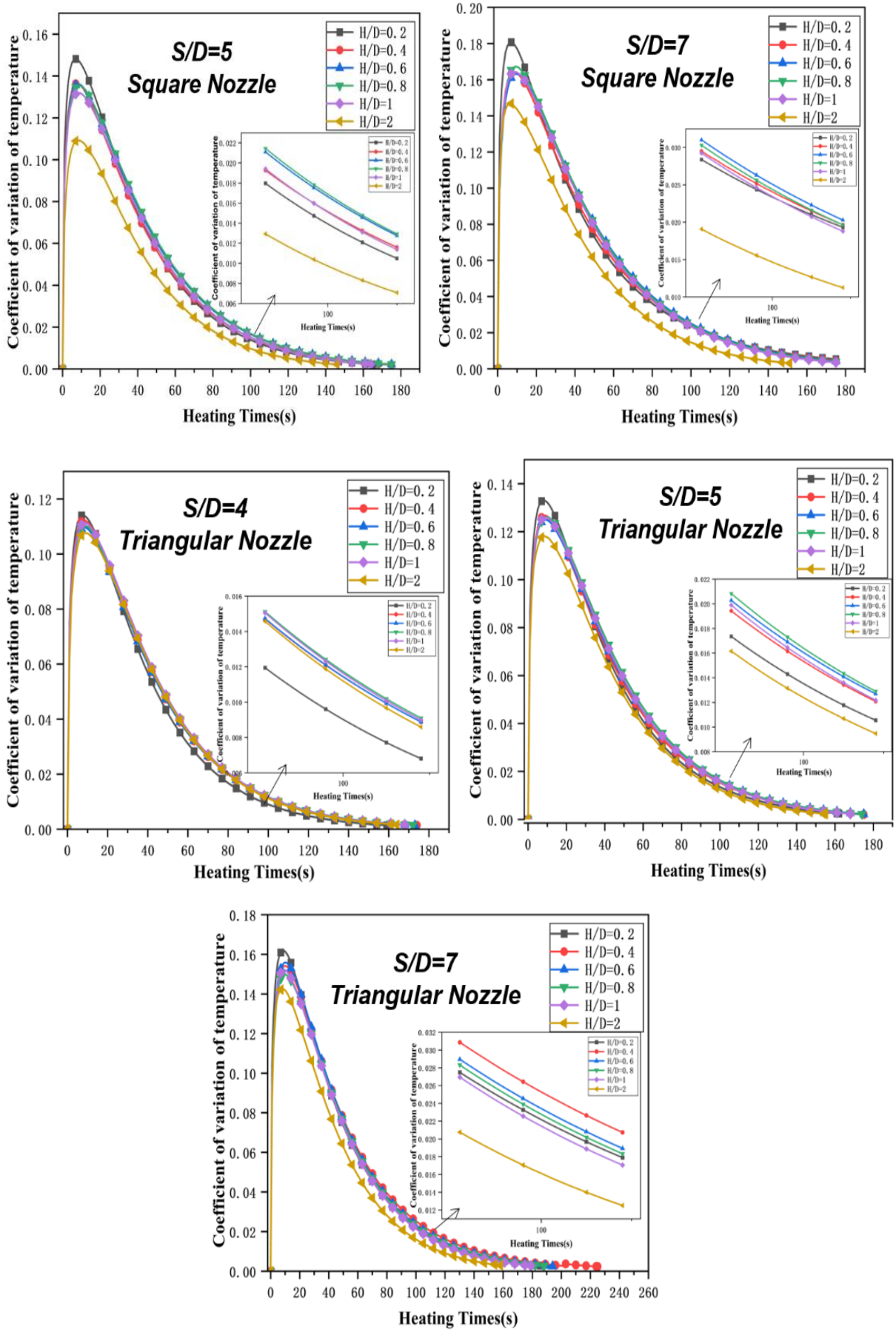

Fig. 12 Study of the transient coefficient of variation of temperature for different nozzle shapes at fixed flow rates: "*S/D*" for 4, 5, 7, "*H/D*" for 0.2-2

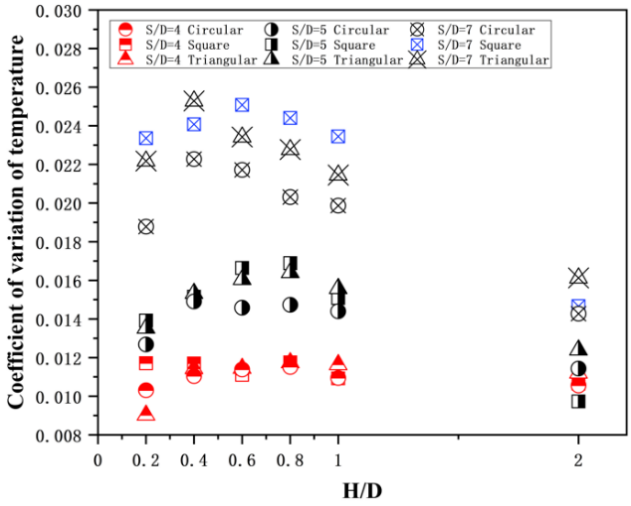

Fig.13 The magnitude of the coefficient of variation of temperature for different jet configurations at the late stage of heating (100 s)

the heat transfer uniformity increased with increasing Re for all three nozzle shapes, although a temporary decline in uniformity occurred during the early stages of heating. The transient trend of the coefficient of variation of temperature followed a consistent pattern across all of the various jet configurations, exhibiting a rapid increase within the initial 10 s followed by a gradual decrease to a stable value. Combined with the results from the coefficient of variation of temperature for the three nozzle shapes at the late stage of heating (100s) in Fig. 11, it is evident that increasing *Re* from 2000 to 6000 greatly enhanced the heat transfer uniformity. This enhancement can be ascribed to the increased turbulence intensity in the wall–jet region and a larger jet impingement area, thereby improving the heat transfer uniformity on the impingement wall. When *Re*≥8000, the heat transfer uniformity slightly improved with increasing *Re*, and the σ_{T,t_j} values for the circular and square nozzles were similar. In addition, the triangular nozzles exhibited the best heat transfer uniformity at *Re*=2000. This was ascribed to the stronger three-dimensional development of triangular jets compared with circular or square jets at lower *Re* values (Singh et al., 2003), leading to a larger heated surface area on the impingement wall. As a result, heat transfer uniformity is improved. For other *Re* values, the circular nozzles gave better heat transfer uniformity, followed by the square nozzles.

As shown in Figs. 12 and 13, at low *H*/*D* values, the heat transfer uniformity worsened with increasing *H*/*D* during the early stage of heating. However, in the late stage of heating (100 s), the heat transfer uniformity always initially deteriorated and then improved with increasing *H*/*D*. Distinct inflection points were observed for the circular and non-circular nozzles, which was attributed to the combined influences of the nozzle shape, nozzle-to-nozzle spacing, and nozzle-to-plate distance on the jet deflection effect. The results are presented in Table 2, and the inflection points all fell within the range of 0.4≤*H*/*D*≤0.8 during the late stage of heating, which renders it challenging to obtain good heat transfer uniformity for jet configurations with these specific nozzle-to-plate distances.

It can also be seen from Figs. 12 and 13 that the heat transfer uniformity for different nozzle shapes improved significantly with decreasing *S*/*D* at a certain mass flow rate. This improvement can be ascribed to the reduction of jet interference before impingement on the plate, leading to a decrease in vortex generation, while enhancing the interaction between jets (Attalla et al., 2017; San & Chen, 2014). In addition, the higher number of nozzles and their close arrangement, which increases the heated surface area on the impingement wall, also contributed to the improved uniformity.

With the larger nozzle-to-nozzle spacings (*S*/*D*≥5), the heat transfer uniformity for the non-circular nozzle is always worse than that of the circular nozzle. However, similar to the circular nozzle, the best heat transfer uniformity is achieved at *H*/*D* = 2, followed by *H*/*D* = 0.2. At the smaller nozzle-to-nozzle spacing (*S*/*D* = 4), where Re is relatively small, the heat transfer uniformity is best at *H*/*D* = 0.2. The heat transfer uniformity of the triangular nozzle is better than the circular nozzle and square nozzle. This is attributed to the superior secondary flow characteristics of triangular nozzles compared to circular and square nozzles, along with the strongest three-dimensional development observed in triangular nozzles (Kim & Park, 2013). Moreover, Singh et al. (2003) reported that non-circular jet flows induce the most significant entrainment and spreading effects, especially in the case of isosceles triangular cross-sections. Consequently, for smaller *S*/*D* and *H*/*D* values, the turbulence intensity within the confined impinging jets intensifies, leading to an increased effective impingement area and thus improved surface temperature uniformity for triangular nozzles. Notably, irrespective of the *S*/*D* value, the square nozzles always afforded the best heat transfer uniformity compared to other corresponding nozzle shapes at *H*/*D* = 2.

During the early stage of heating, the optimal heat transfer uniformity was observed for the triangular

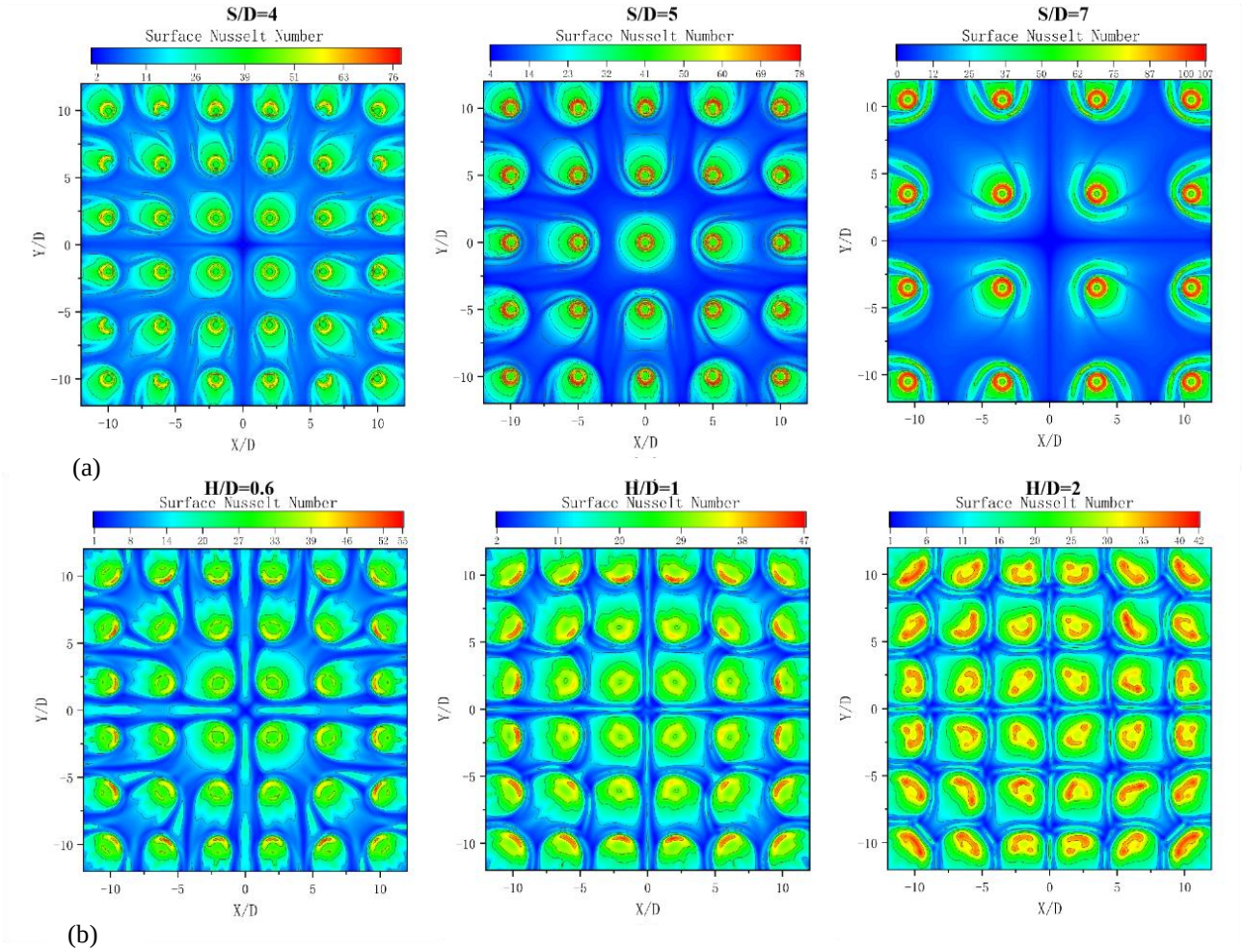

Fig. 14 Heated to 20 s. (a) *H/D* = 0.2, surface Nusselt number contour of the circular nozzle at different *S/D* (b) *S/D* = 4, surface Nusselt number contour of the circular nozzle at different *H/D*

nozzles, followed by the square nozzles. In the late heating stage, upon examining Table 2, we observe that at small *H/D*, good heat transfer uniformity is only achieved at *H/D* = 0.2 or *H/D* = 2. Moreover, smaller nozzle-to-nozzle spacings exhibited better heat transfer uniformity; thus, at *H/D*=0.2 and *S/D*=4, the triangular nozzles provided superior heat transfer uniformity throughout the heating process.

5.3 Surface Nusselt Number Distribution

Figures. 14, 15, and 16 display the contours during square-array jet impingement using different nozzle shapes with heating for 20 s. The results consistently indicated a "horseshoe" shape around the array jet impingement hole, especially near the exit area. This observation demonstrates periodic repeatability, suggesting a symmetrical distribution of the surface *Nu* on the impingement wall. Figures. 15 and 16 show the axis switching of the jet caused by the presence of counterflow vortices at the corners of the non-circular nozzles. For triangular nozzles located near the center of the surface, a significant axis-switching phenomenon occurred with an axis switching of 180°, whereas the square nozzles exhibited an axis switching of 90°. This behavior is closely related to the evolution of non-circular jets and the changes in swirling vortices (Kim & Park, 2013; Vinze et al., 2016). However, the axis-switching phenomenon near the jet orifice at the exit was not pronounced because the interactions between the non-circular impinging jets and crossflow affected the evolution of the jets, resulting in less apparent axis switching in the downstream region. Furthermore, the overall surface *Nu* contours for the circular nozzles had a slightly deeper color than those for the non-circular nozzles at larger *S/D* and *H/D* values, which was attributable to the higher decay rate of non-circular jets compared with circular jets (Singh et al., 2003; Kim & Park, 2013; Vinze et al., 2016).

The contour plots of Nusselt numbers obtained from our study in Figs. 14, 15, and 16 exhibit a strong correlation with the results reported by Vinze et al. (2016) at the corresponding *H/D*. The local maximum for each of the non-circular nozzles occurred at the apex, with the triangular nozzles displaying the highest local maximum, followed by the square nozzles. This can be attributed to the increased entrainment and mixing with the surrounding fluid that non-circular jets provide, along with their stronger secondary flows (Kim & Park, 2013). Particularly at smaller *H/D*, there is a significant enhancement in the local turbulence intensity within the apex region of non-circular jets. In contrast, the local Nusselt number distribution of a single circular nozzle has

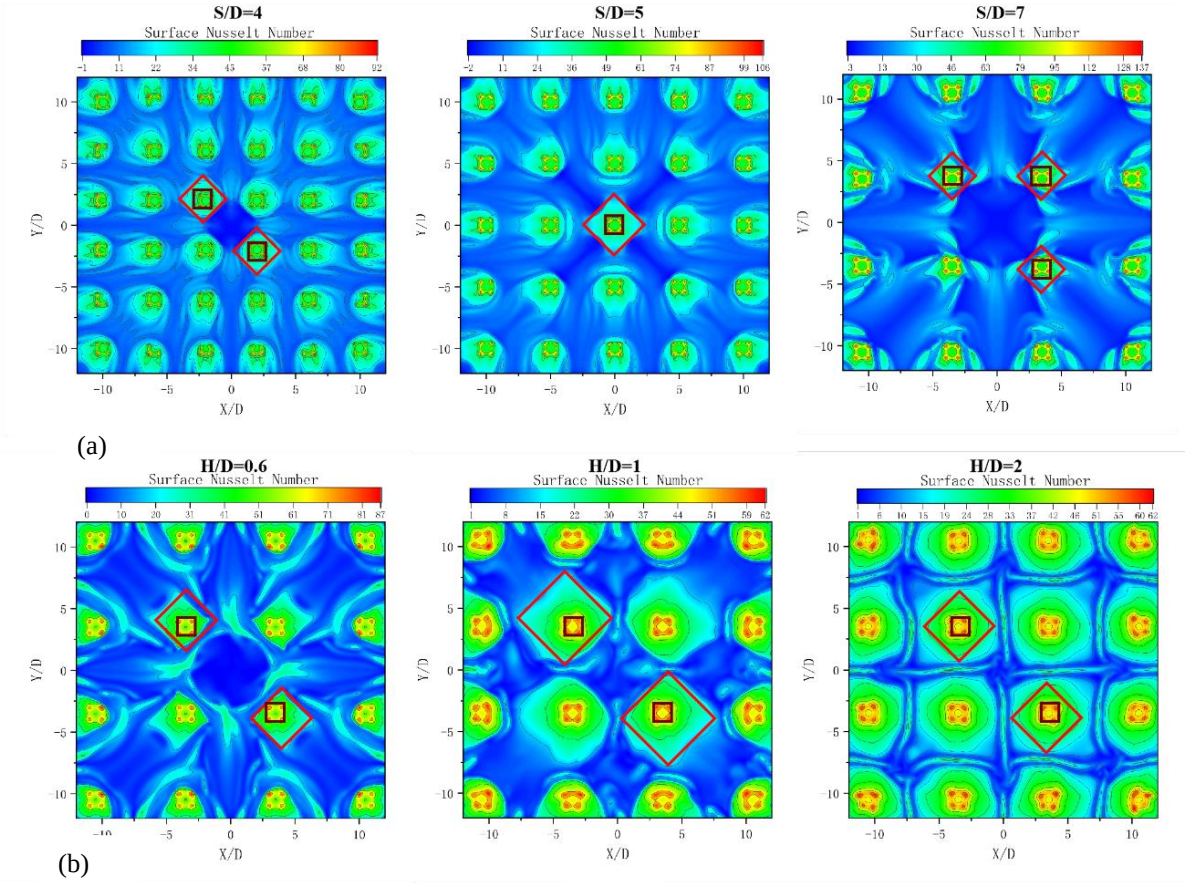

Fig. 15 Heated to 20 s. (a) *H/D* = 0.2, surface Nusselt number contour of the square nozzle at different *S/D* (b) *S/D* = 4, surface Nusselt number contour of the square nozzle at different *H/D*

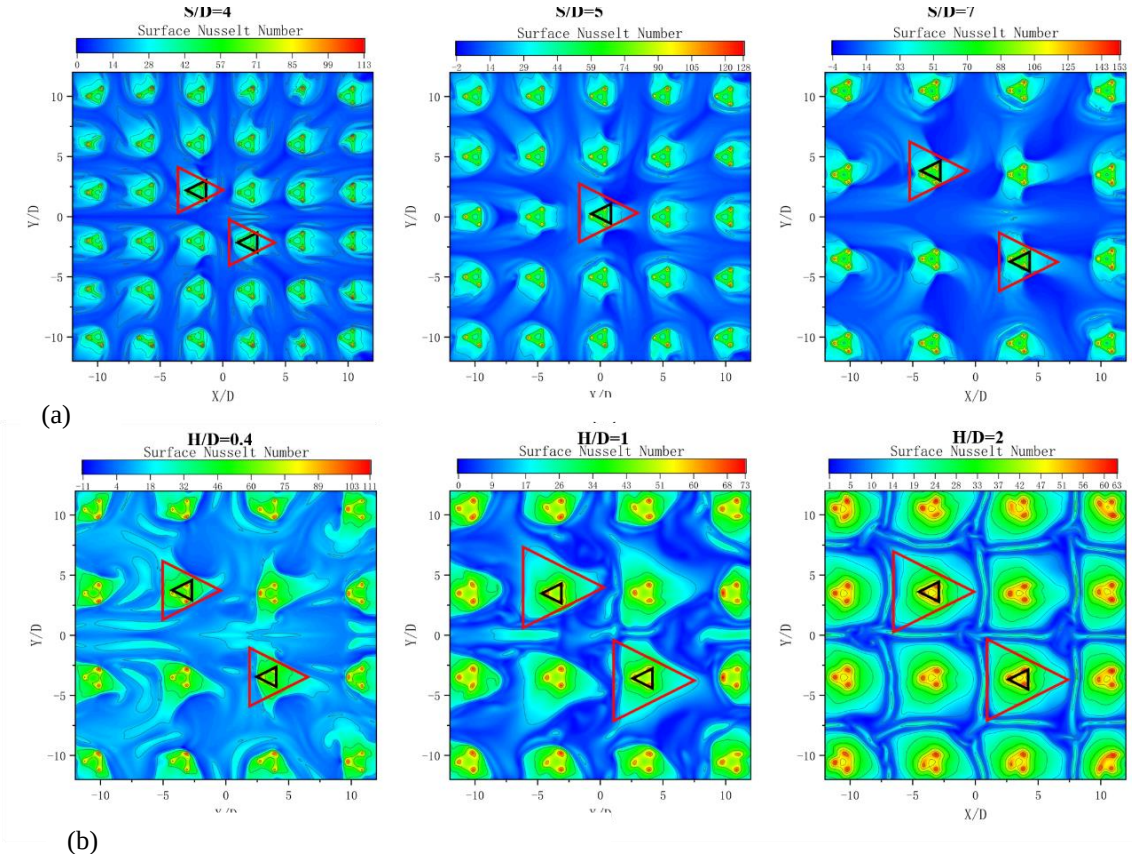

Fig. 16 Heated to 20 s. (a) *H/D* = 0.2, surface Nusselt number contour of the triangular nozzle at different *S/D* (b) *S/D* = 4, surface Nusselt number contour of the triangular nozzle at different *H/D*

the largest local Nusselt number in the stationary region and gradually decreases towards the surrounding.

When $H/D \geq 0.4$, the peak position of the local Nusselt number of every single hole gradually moved closer to the center of the impingement wall. This was caused by the influence of crossflow effects, where a dense array of orifices and confined impinging jets result in intensified interactions between the impinging jets and their surrounding crossflow. These interactions affect the heat transfer in the downstream region. At H/D=0.2, we also observed that the peak position of the local Nusselt number for each hole shifted slightly toward the exit flow direction, with minimal influence from the crossflow. This observation further signifies the existence of an inflection point for small nozzle-to-plate distances.

Figures. 14 a), 15 a), and 16 a) present a clear trend: for different nozzle shapes, the local maximum Nusselt number at the jet impingement wall increases with increasing S/D. San and Chen (2014), Attalla et al. (2017), and Behbahani and Goldstein (1983) found that the surface local maximum Nusselt number is attributed to the jet interaction. At smaller S/D, jet interference prior to impingement caused a decrease in heat transfer. At larger S/D, the nozzles within the square array could be regarded as individual jets and each nozzle had a larger incident Re, resulting in higher local Nusselt numbers. This phenomenon also accounts for the significant axis switching observed for the non-circular nozzles at larger S/D. By combining the analysis of the local heat transfer with the variation of H/D shown in Figs. 14(b), 15(b), and 16(b), it was observed that at small H/D values the local maximum Nusselt numbers decreased with increasing H/D. For H/D values between 0.2 and 1, there were large differences in the local maximum. Specifically, the difference was 56% for the circular nozzles at S/D=7, 36% for the triangular nozzles at S/D=4, and 33% for the square nozzles at S/D=4. This can be ascribed to variations in the inherent core length and three-dimensional development of the jets obtained using different nozzle shapes (Kim & Park, 2013). It was also found that there exists the potential for negative heat flow during the heating process using non-circular nozzles at larger S/D and small H/D, which is the main reason for their poor heat transfer rate and uniformity.

6. CONCLUSION

For the large-size, ultra-thin physical tempering process, this paper designs nozzles with three cross-sectional shapes: circular, square, and triangular. The effects of variations in the Re, S/D, and H/D values were examined to assess the influence of these parameters on the heat transfer rate and heat transfer uniformity of the system. The following conclusions were obtained:

(1) At small H/D values, the influences of changes in Re, H/D, and S/D on the heat transfer performance for non-circular nozzles were comparable to those observed for circular nozzles.

The heat transfer rate increased with increasing Re, resulting in an improvement in the transient heat transfer uniformity.

A high heat transfer rate and favorable heat transfer uniformity were achieved exclusively at H/D=0.2 or 2, and the influence of crossflow was minor at H/D=0.2. As H/D increased, the $\overline{Nu}$ at the impingement wall first diminished then increased, with the inflection point occurring at H/D=0.4. In the later stage of heating, the heat transfer uniformity initially worsened and then improved with increasing H/D, with the inflection point occurring within the range of $0.4 \leq H/D \leq 0.8$.

At a certain mass flow rate, the jet impingement heat transfer rate gradually deteriorated with decreasing S/D, while the heat transfer uniformity significantly increased.

(2) In addition, the non-circular nozzles exhibit a higher local maximum Nusselt number than the circular ones. Notably, significant axis switching was observed only around the impingement hole near the center of the impingement wall, with axis switching of 180° for the triangular nozzle and 45° for the square nozzle. At specific jet configurations, square nozzles afforded superior heat transfer rates at smaller S/D, and larger nozzle-to-plate distances ($1 \leq H/D \leq 2$). They also provided better heat transfer uniformity at H/D=2. At smaller values of S/D, H/D=0.2, and lower Re values, triangular nozzles exhibited the best heat transfer uniformity throughout the heating process. For the remaining jet configurations, the circular nozzles performed better than the corresponding non-circular nozzles.

(3) Under the same conditions, appropriately increasing Re helped to reduce the glass heating time and significantly improved the heat transfer uniformity. At a certain mass flow rate, the heat transfer uniformity of the jet array during the physical tempering of ultrathin glass can be improved by reducing the jet spacing S/D. Especially using H/D=0.2 is selected in the low H/D range, the triangular and circular jets can further shorten the glass heating time and improve the heat transfer uniformity.

The results obtained in this study provide important insights for optimizing the physical tempering process for ultrathin glass and offer more efficient methods for uniform heat transfer in the high-tech and energy industries. In the gas-suspended glass physical temper, there is a strong requirement for a uniform pressure distribution on the glass surface subjected to jet impingement heating. In the future, we will further explore the distribution patterns of the wall pressure under low jet heights for both circular and non-circular jets. This is anticipated to prove valuable for further improving the process design and enhancing the flatness of glass surfaces.

ACKNOWLEDGEMENTS

This work was supported by the National Natural Science Foundation of China (Grant No.52275191,92248301 and 51905049), the Qing Lan Project of Jiangsu Province, and the 333 Project of Jiangsu Province.

CONFLICT OF INTEREST

The author(s) declared no potential conflicts of interest with respect to the research, authorship and publication of this article.

AUTHORS CONTRIBUTION

Zhijie Li: Conceptualization, Methodology, Formal analysis, Writing - original draft, Writing - review and editing. **Guanggui Cheng**: Conceptualization, Writing - original draft, Writing - review and editing， Resources. **Keqian Zhu:** Writing - review and editing, Software， Investigation. **Zhongqiang Zhang:** Supervision, Investigation. **Junliang Lin:** Supervision， Validation. **Junliang Lin:** Supervision， Validation. **Jianning Ding:** Supervision, Project administration.

REFERENCES

Attalla, M., Maghrabie, H. M., Qayyum, A., Al-Hasnawi, A. G., & Specht, E. (2017). Influence of the nozzle shape on heat transfer uniformity for in-line array of impinging air jets. *Applied Thermal Engineering, 120*, 160-169 . https://doi.org/10.1016/j.applthermaleng.2017.03.134

Behbahani, A. I., & Goldstein, R. J. (1983). Local heat transfer to staggered arrays of impinging circular air jets. *Journal of Engineering for Power, 105*(2), 354-360 .https://doi.org/10.1115/1.3227423

Bhagwat, A. B., & Sridharan, A. (2016). Convective heat transfer from a heated plate to the orthogonally impinging air jet. *Journal of Thermal Science and Engineering Applications, 8*(4) . https://doi.org/10.1115/1.4034058

Bijarchi, M. A., Eghtesad, A., Afshin, H., & Shafii, M. B. (2019). Obtaining uniform cooling on a hot surface by a novel swinging slot impinging jet. *Applied Thermal Engineering, 150*, 781-790 . https://doi.org/https://doi.org/10.1016/j.applthermaleng.2019.01.037

Choo, K., Friedrich, B. K., Glaspell, A. W., & Schilling, K. A. (2016). The influence of nozzle-to-plate spacing on heat transfer and fluid flow of submerged jet impingement. *International Journal of Heat and Mass Transfer, 97*, 66-69 . https://doi.org/10.1016/j.ijheatmasstransfer.2016.01.060

Culun, P., Celik, N., & Pihtili, K. (2018). Effects of design parameters on a multi jet impinging heat transfer. *Alexandria Engineering Journal, 57*(4), 4255-4266 . https://doi.org/10.1016/j.aej.2018.01.022

Ekkad, S. V., & Singh, P. (2021). A Modern review on jet impingement heat transfer methods. *Journal of Heat Transfer, 143*(6) .https://doi.org/10.1115/1.4049496

Ferrari, J., Lior, N., & Slycke, J. (2003). An evaluation of gas quenching of steel rings by multiple-jet impingement. *Journal of Materials Processing Technology, 136*(1), 190-201 . https://doi.org/10.1016/s0924-0136(03)00158-4

Glaspell, A. W., Rouse, V. J., Friedrich, B. K., & Choo, K. (2019). Heat transfer and hydrodynamics of air assisted free water jet impingement at low nozzle-to-surface distances. *International Journal of Heat and Mass Transfer, 132*, 138-142 . https://doi.org/10.1016/j.ijheatmasstransfer.2018.11.173

Huber, A. M., & Viskanta, R. (1994). Effect of jet-jet spacing on convective heat transfer to confined, impinging arrays of axisymmetric air jets. *International Journal of Heat and Mass Transfer, 37*(18), 2859-2869 .https://doi.org/10.1016/0017-9310(94)90340-9

Ichikawa, Y., Motosuke, M., Kameya, Y., Yamamoto, M., & Honami, S. (2016). Three-dimensional flow characterization of a square array of multiple circular impinging jets using stereoscopic PIV and heat transfer relation. *Journal of Visualization, 19*(1), 89-101. https://doi.org/10.1007/s12650-015-0296-8

Ikhlaq, M., Al-Abdeli, Y. M., & Khiadani, M. (2019). Transient heat transfer characteristics of swirling and non-swirling turbulent impinging jets. *Experimental Thermal and Fluid Science, 109*, 109917. https://doi.org/10.1016/j.expthermflusci.2019.109917

Jensen, M. V., & Walther, J. H. (2013). Numerical Analysis of Jet Impingement Heat Transfer at High Jet Reynolds Number and Large Temperature Difference. *Heat Transfer Engineering, 34*(10), 801-809. https://doi.org/10.1080/01457632.2012.746153

Kim, W. H., & Park, T. S. (2013). Effects of noncircular inlet on the flow structures in turbulent jets. *Journal of Applied Mathematics and Physics, 1*(6), 37-42. https://doi.org/10.4236/jamp.2013.16008

Lee, J., Ren, Z., Haegele, J., Potts, G., Sik Jin, J., Ligrani, P., Fox, M. D. & Moon, H. K. (2013). Effects of Jet-to-target plate distance and reynolds number on jet array impingement heat transfer. *Journal of Turbomachinery, 136*(5). https://doi.org/10.1115/1.4025228

Lytle, D., & Webb, B. W. (1994). Air jet impingement heat transfer at low nozzle-plate spacings. *International Journal of Heat and Mass Transfer, 37*(12), 1687-1697. https://doi.org/10.1016/0017-9310(94)90059-0

Nguyen, C. T., Galanis, N., Polidori, G., Fohanno, S., Popa, C. V., & Le Bechec, A. (2009). An experimental study of a confined and submerged impinging jet heat transfer using Al2O3-water nanofluid. *International Journal of Thermal Sciences, 48*(2), 401-411 . https://doi.org/10.1016/j.ijthermalsci.2008.10.007

San, J. Y., & Chen, J. J. (2014). Effects of jet-to-jet spacing and jet height on heat transfer characteristics of an impinging jet array. *International Journal of*

Heat and Mass Transfer, *71*, 8-17. https://doi.org/10.1016/j.ijheatmasstransfer.2013.11.079

San, J. Y., & Lai, M. D. (2001). Optimum jet-to-jet spacing of heat transfer for staggered arrays of impinging air jets. *International Journal of Heat and Mass Transfer*, *44*(21), 3997-4007. https://doi.org/10.1016/s0017-9310(01)00043-6

Singh, A., & Prasad, B. V. S. S. S. (2020). *Heat Transfer and flow visualization of equilaterally staggered jet arrangement on a flat surface*. https://doi.org/10.1115/GT2020-14196

Singh, G., Sundararajan, T., & Bhaskaran, K. A. (2003). Mixing and entrainment characteristics of circular and noncircular confined jets. *Journal of Fluids Engineering*, *125*(5), 835-842. https://doi.org/10.1115/1.1595676

Singh, P., Grover, N. K., Agarwal, V., Sharma, S., Singh, J., Sadeghzadeh, M., & Issakhov, A. (2021). Computational Fluid dynamics analysis of impingement heat transfer in an inline array of multiple jets. *Mathematical Problems in Engineering*, *2021*, 6668942. https://doi.org/10.1155/2021/6668942

Siw, S. C., Miller, N., Alvin, M., & Chyu, M. (2016). Heat transfer performance of internal cooling channel with single-row jet impingement array by varying flow rates. *Journal of Thermal Science and Engineering Applications*, *9*(1). https://doi.org/10.1115/1.4034686

Tang, Z. G., Deng, F., Wang, S. C., & Cheng, J. P. (2020). Numerical Simulation of flow and heat transfer characteristics of a liquid jet impinging on a cylindrical cavity heat sink. *Journal of Applied Fluid Mechanics*, *14*(3), 723-732. https://doi.org/10.47176/jafm.14.03.31945

Vinze, R., Chandel, S., Limaye, M. D., & Prabhu, S. V. (2016). Influence of jet temperature and nozzle shape on the heat transfer distribution between a smooth plate and impinging air jets. *International Journal of Thermal Sciences*, *99*, 136-151. https://doi.org/10.1016/j.ijthermalsci.2015.08.009

Xing, Y., & Weigand, B. (2013). Optimum jet-to-plate spacing of inline impingement heat transfer for different crossflow schemes. *Journal of Heat Transfer*, *135*(7). https://doi.org/10.1115/1.4023562

Yang, D., Qiu, M., Wu, H., Li, Y., Jiang, Z., & Huang, K. (2023). Temperature uniformity characteristics of array jet impingement cooling with the maximum cross-flow scheme. *International Journal of Thermal Sciences*, *187*, 108161. https://doi.org/10.1016/j.ijthermalsci.2023.108161

Yang, H., Liu, F., Duan, R., Shi, F., & Tian, L. (2022). Spray cooling heat transfer during glass tempering process and influencing factors on the quality of tempered glass. *International Journal of Thermal Sciences*, *175*, 107475. https://doi.org/10.1016/j.ijthermalsci.2022.107475

Yazici, H., Akcay, M., Golcu, M., Koseoglu, M. F., & Sekmen, Y. (2015). Experimental investigation of transient temperature distribution and heat transfer by jet impingement in glass tempering processing.*Iranian Journal of Science and Technology Transactions of Mechanical Engineering*, *39*(M2), 337-349. https://doi.org/10.22099/ijstm.2015.3244

Yu, P., Zhu, K., Shi, Q., Yuan, N., & Ding, J. (2017a). Transient heat transfer characteristics of small jet impingement on high-temperature flat plate. *International Journal of Heat and Mass Transfer*, *114*, 981-991. https://doi.org/10.1016/j.ijheatmasstransfer.2017.06.112

Yu, P., Zhu, K., Sun, T., Yuan, N., & Ding, J. (2017b). Heat transfer rate and uniformity of mist flow jet impingement for glass tempering. *International Journal of Heat and Mass Transfer*, *115*, 368-378. https://doi.org/10.1016/j.ijheatmasstransfer.2017.08.065

Zhang, H., Jia, L., Cui, L. S., & Li, C. H. (2020). Investigation on the gas jet flow performance confined in round pipe. *Journal of Applied Fluid Mechanics*, *14*(3), 669-680. https://doi.org/10.47176/jafm.14.03.31847

Zhao, W., Kumar, K., & Mujumdar, A. S. (2004). Flow and heat transfer characteristics of confined noncircular turbulent impinging jets. *Drying Technology*, *22*(9), 2027-2049. https://doi.org/10.1081/DRT-200034239

Zhou, T., Xu, D., Chen, J., Cao, C., & Ye, T. (2016). Numerical analysis of turbulent round jet impingement heat transfer at high temperature difference. *Applied Thermal Engineering*, *100*, 55-61. https://doi.org/10.1016/j.applthermaleng.2016.02.006

Zhu, K., Yu, P., Yuan, N., & Ding, J. (2018). Transient heat transfer characteristics of array-jet impingement on high-temperature flat plate at low jet-to-plate distances. *International Journal of Heat and Mass Transfer*, *127*, 413-425. https://doi.org/10.1016/j.ijheatmasstransfer.2018.07.099

Zuckerman, N., & Lior, N. (2006). Jet Impingement Heat Transfer: Physics, Correlations, and Numerical Modeling. In G. A. Greene, J. P. Hartnett, A. Bar-Cohen & Y. I. Cho (Eds.), *Advances in Heat Transfer* (Vol. 39, pp. 565-631), Elsevier. https://doi.org/10.1016/S0065-2717(06)39006-5